Supplementary Information

Quantum-precision-spectroscopy metrology of vacuum Rabi splitting in plasmon-single-emitter strong coupling

Shihao Feng[1,2,7], Xinyi Fan[1,7], Qiang Li[3,7], Wen-Jie Zhou[4,7], Ting Luo[1], De-Ke Chen[5], Guanqian Wu[1], Wan-Ying Li[1], Jia Wang[1], Longhui Du[1], Haowen Zhang[1], Yanmin Kuang[1], Bo Wang[6], Wei Li[5,*], Lijun Guo[1,*], Lin Wu[4,*], Renming Liu[1,2,*], and Xue-Hua Wang[5]

[1]*Henan Key Laboratory of High Efficiency Energy Conversion Science and Technology, Henan International Joint Laboratory of New Energy Materials and Devices, School of Physics and Electronics, Henan University, Kaifeng 475004, China.*

[2]*Institute of Quantum Materials and Physics, Henan Academy of Sciences, Zhengzhou 450046, China.*

[3]*School of Physics, Henan Normal University, Xinxiang 453007, China.*

[4]*Department of Science, Mathematics and Technology, Singapore University of Technology and Design, 8 Somapah Road, Singapore 487372, Republic of Singapore.*

[5]*State Key Laboratory of Optoelectronic Materials and Technologies, School of Physics, Sun Yat-sen University, Guangzhou 510275, China.*

[6]*Future Technology, Henan University, Zhengzhou 450046, China.*

[7]*These authors contributed equally: Shihao Feng, Xinyi Fan, Qiang Li, Wen-Jie Zhou*

***Corresponding to:** *liwei373@mail.sysu.edu.cn; juneguo@henu.edu.cn; lin_wu@sutd.edu.sg*; and *liurm@henu.edu.cn*

Contents

Supplementary Note 1: Quantum mechanical model for plasmon-single-emitter strong coupling

The strong coupling between a plasmonic nanocavity and a single quantum emitter was described using a fully quantum mechanical framework. Specifically, the plasmon mode supported by the nanocavity is represented by bosonic annihilation and creation operators, while the emitter is modeled as a fermionic two-level system consisting of ground and excited states. The Hamiltonian of this coupling system can be written as[1,2]

$$H = \varepsilon_p p^+ p + \varepsilon_e e^+ e - g[p^+ e + e^+ p] + H_{decay} \quad \text{(S1)}$$

where $e(e^+)$ is the annihilation (creation) operator for the quantum emitter with energy of ε_e, and $p(p^+)$ is the annihilation (creation) operator of the plasmon mode with

energy of ε_p. g is the coupling coefficient between the plasmon mode and the emitter, which can be calculated using the following Supplementary Eq. (2),

$$g = \frac{\varepsilon_e}{\sqrt{2\epsilon_0 \varepsilon_p V_{eff}}} \boldsymbol{\mu}_e \cdot \boldsymbol{f}_p(\boldsymbol{r}) \ , \tag{S2}$$

where ϵ_0 is the free-space permittivity, $V_{eff} = n^2 \times V_m$ is the effective mode volume of the Au NDC, n is the refractive index, V_m is the and mode volume, $\boldsymbol{\mu_e}$ is the transition dipole moment of the quantum emitter, $\boldsymbol{f}_p(\boldsymbol{r}) = \boldsymbol{E}_p(\boldsymbol{r})/|\boldsymbol{E}_p(\boldsymbol{r})|_{max}$ is the normalized electric field (EF) of the plasmon mode at the position of $\boldsymbol{r}$. To account for the finite lifetimes of both the plasmon and emitter, the Hamiltonian in Supplementary Eq. (1) incorporates inelastic interaction Hamiltonian (H_{decay}) between the two coupled subsystems and their environment, modeled as a continuum of bosonic modes,

$$\begin{aligned} H_{decay} = & \int d\omega \hbar\omega f_p^+(\omega) f_p(\omega) + \int d\omega \hbar\omega f_e^+(\omega) f_e(\omega) \\ & - \int d\omega \left[v_p(\omega) f_p(\omega) p^+ + v_p^*(\omega) f_p^+(\omega) p \right] \\ & - \int d\omega [v_e(\omega) f_e(\omega) e^+ + v_e^*(\omega) f_e^+(\omega) e], \end{aligned} \tag{S3}$$

where $f_e(\omega)$ ($f_e^+(\omega)$) is the annihilation (creation) operator of the continuum modes that couple to the emitter, and the corresponding coupling strength is $v_e(\omega)$; $f_p(\omega)$ ($f_p^+(\omega)$) is the annihilation (creation) operator of the continuum modes that couple to the plasmon mode, the corresponding coupling coefficient is $v_p(\omega)$.

Assuming that only plasmons coupled efficiently to the external photons, the absorption spectrum observed from the plasmon channel can be deduced based on Zubarev's Green function[3] $\langle\langle p \ ; \ p^+ \rangle\rangle_{\omega + i0^+}$ as,

$$\zeta(\omega) \propto -Im\left\{ \langle\langle p \ ; \ p^+ \rangle\rangle_{\omega + i0^+} \right\} = -Im\left\{ \hbar\omega - \varepsilon_p + \delta\varepsilon_p + i\frac{\Gamma_p}{2} - \frac{g^2}{\hbar\omega - \varepsilon_e + \left(\delta\varepsilon_e + i\frac{\Gamma_e}{2}\right)} \right\}^{-1} \tag{S4}$$

where $\delta\varepsilon_p$ ($\delta\varepsilon_e$) and Γ_p (Γ_e) are the energy shift and the damping linewidth (i.e., full width at half maximum, FWHM) of the plasmon mode and the emitter induced by the reservoir field, respectively. The energy shifts $\delta\varepsilon_p$ and $\delta\varepsilon_e$ can be accounted by renormalizing the transition energies ε_p and ε_e, respectively. Thus,

$$\zeta(\omega) \propto -Im\frac{(\hbar\omega-\varepsilon_e+i\Gamma_e/2)}{(\hbar\omega-\varepsilon_p+i\Gamma_p/2)\cdot(\hbar\omega-\varepsilon_e+i\Gamma_e/2)-g^2} \quad \text{(S5)}$$

It should be noted that the scattering spectrum of the strongly coupled system—mainly arising from the plasmonic channel and commonly probed in experiments—can also be described by Supplementary Eq. (5) when measuring the optical response from the same plasmon-channel, provided we ignore differences in intensity[4]. At resonance, where $\varepsilon_p = \varepsilon_e$, the analytical expression for the spectral splitting (SS) observed in the absorption/scattering via the plasmonic channel, denoted as Ω_{SS}^{p}, can be derived by solving $\frac{d\zeta(\omega)}{d\omega} = 0$, yielding

$$\Omega_{SS}^{p} = 2\sqrt{g(1+\Gamma_e/\Gamma_p)\cdot(g^2+\Gamma_e\Gamma_p/4)^{1/2}-(g^2+\Gamma_e\Gamma_p/4)\cdot\Gamma_e/\Gamma_p}\ , \quad \text{(S6)}$$

with the corresponding critical coupling criterion given by,

$$g^2 > \frac{\Gamma_e^2}{8(1+\Gamma_p/2\Gamma_e)} \quad \text{(S7)}$$

Supplementary Note 2: Fabrication and spectral characterization of CB[7]@single MB emitters

To fabricate a single-molecule emitter, methylene blue (MB) molecules were employed. Host-guest chemistry with cucurbit[7]uril(CB[7]) was utilized to prevent dye aggregation and ensure isolated emitter formation. In specific, an aqueous CB[7] solution (2 mL, 1.0×10^{-7} M) was prepared in a thermostatic water bath at 50 °C. Then, 1 mL of MB aqueous solution (1.0×10^{-7} M) was added and thoroughly mixed under ultrasonication for 10 min, yielding a molar ratio of MB: CB[7] = 1: 2. This procedure resulted in the encapsulation of individual MB molecules within separate CB[7] cavities, producing the CB[7]@single MB emitter complex.

The integration of a single MB molecule inside the CB[7] can be confirmed by the absorption spectroscopy. As illustrated in Supplementary Fig. S5, the absorption of MB dimers (indicated by the minor shoulder peak at 612 nm on the black curve) is markedly reduced and nearly vanishes upon mixing MB with CB[7] in a 1:2 molar ratio (the blue curve in Supplementary Fig. S5). We note that the size of the MB dimer is too large to

be encapsulated within a single CB[7] molecule. The absorption spectrum of CB[7]@single MB emitters in the mixture was fitted to display the transition energy and damping linewidth of single MB emitters, showing a spectral FWHM of about 70 meV (the dashed green line in Supplementary Fig. S5). Next, we precisely integrate a single CB[7]@single MB emitter at the gap center of a gold nanodimer cavity (Au NDC), where the electric field (EF) intensity is the maximum (Methods in main text and Supplementary Fig. S2d).

Supplementary Note 3: Calculation of mode volume (V_m) from Purcell factor (F_p)

Firstly, the standard Purcell factor (F_p) calculation looks at the spontaneous emission rate of a classical electric dipole at the gap center of the Au NDC. We use the three-dimensional finite element method (3D-FEM) to extract this emission rate as well as to quantify the cavity Q factor. A typical simulation of the Au NDC, comprising two 84 nm Au nanoparticles spaced 0.9 nm apart and positioned on a bulk SiO_2 substrate, yields a spectrum for the spontaneous emission rate, as shown in Supplementary Fig. S7. In calculations, the CB[7]@single MB emitter embedded in the gap of the Au NDC was modeled as a dielectric cylinder (0.75 nm in radius and 0.9 nm in length) with a refractive index of 1.4, and the mesh was set at 0.1 nm in the nanogap. Our calculations show that the F_p in the gap center is up to $F_p \sim 1.42 \times 10^6$ at the resonant wavelength of λ = 660 nm (Supplementary Fig. S7). Based on this Purcell factor, we can calculate the Q factor of the Au NDC at this resonant wavelength, yielding Q = 9.54. Since the Purcell factor is defined as,

$$F_p = \frac{3}{4\pi^2}\frac{Q}{V_m}\left(\frac{\lambda}{n}\right)^3, \quad \text{(S8)}$$

so we can extract the V_m at resonant wavelength (660 nm) of V_m= 53.5 nm^3, agreeing well with that calculated using the approach based on equation (5) in the Methods section of the main text.

Supplementary Note 4: Numerical simulations

The scattering spectra and EF simulations of the Au NDC on both bulk SiO_2 and Si/SiO_2 photonic substrates were carried out using 3D-FEM. The boundary conditions in these simulations are consistent with those applied in the V_m calculations described in the Methods section of the main text. In simulations, the Au NDCs were fixed on the surface of the SiO_2 (or Si/SiO_2) substrates, and each Au NDC was constructed from two identical Au nanospheres, each with a radius of 42 nm. The gap distance between the two nanospheres was set at 0.9 nm, which equals the thickness of the CB[7] linker molecule. The dispersion data for Si and SiO_2 are derived from experimentally measured refractive indices reported by Aspens & Studna (1983)[5] for Si and Rodríguez-de Marcos et al. (2016)[6] for SiO_2, respectively. The permittivity of gold is taken from experimental measurements performed by Johnson and Christy[7]. To account for the integration of a single CB[7] molecule into the Au NDC gap in the experimental configuration, a dielectric cylinder was introduced in the gap region, as described in Supplementary Note 3. To calculate the scattering spectra, we integrated the power flow radiating from the surface of the Au NDC and normalized the result to the intensity of the incident field (I_0).

Supplementary Note 5: Photobleaching of the strongly coupled Au NDC/CB[7]@single MB systems

It is established that laser illumination of plasmon-dye-molecule coupled systems induces photobleaching, even at low intensities and short exposure durations[2,8,9]. In our study, we employed this effect to destroy exciton states in Au NDC/CB[7]@MB hybrids using a 633 nm pump laser. The resulting transparency dips in SS were significantly attenuated or entirely eliminated under a relatively weak irradiance (10 $\mu W/\mu m^2$ for 5 min). This bleaching behavior confirms that the observed SS in Fig. 3e of the main text and Supplementary Fig. S10 arise from strong coupling between MB-molecule excitons and Au NDCs.

Supplementary Note 6: Materials and Methods

Supplementary Note 6.1: Materials

Gold (III) chloride trihydrate ($HAuCl_4 \cdot 3H_2O$, >99%), silver nitrate ($AgNO_3$, 99.8%), sodium citrate ($C_6H_5O_7Na_3 \cdot 2H_2O$, 99%), Sodium borohydride ($NaBH_4$, 99%), L-ascorbic acid ($C_6H_8O_6$, >99%), cetyltrimethylammonium bromide (CTAB, ⩾99%), potassium iodide (KI, 99%), sodium hydroxide (NaOH, 99.8%) and sodium chloride (NaCl, 99.5%), Cucurbit[7]urils ($C_{42}H_{42}N_{28}O_{14}$, >99.5%) and methylene blue ($C_{16}H_{18}ClN_3S$, 95%) were purchased from Sigma Aldrich and used as received. In all experiments, we used deionized water with a resistivity of 18.25 MΩ·cm.

Supplementary Note 6.2: Synthesis of Au nanoparticles

Highly purified Au nanoparticles were synthesized according to the following methods[10,11]. In experiments, all glassware was firstly cleaned with aqua regia (3:1 ratio by volume of HCl and HNO_3) and thoroughly rinsed with deionized water. Subsequently, Au nanocrystal seeds were synthesized by reducing $HAuCl_4$ (0.01 M, 2 mL) with freshly prepared ice-cold aqueous $NaBH_4$ (0.1 M, 1 mL) in deionized water (36 mL) under rapid stirring for 1 min. The mixture was aged at 35 ℃ for 4 h to hydrolyze any unreacted $NaBH_4$, yielding Au seeds with an average size of approximately 2 nm. Then, three distinct growth solutions (A, B, and C) were then prepared for seed-mediated nanoparticle growth. Solutions A and B had identical compositions, each containing NaOH (0.05 mL, 0.1 M), ascorbic acid (0.05 mL, 0.1 M), KI (4.5 μL, 0.1 M), CTAB (9.0 mL, 0.05 M), and $HAuCl_4$ (0.25 mL, 10 mM). Solution C consisted of NaOH (0.25 mL, 0.1 M), ascorbic acid (0.25 mL, 0.1 M), KI (23 μL, 0.1 M), CTAB (45 mL, 0.05 M), and $HAuCl_4$ (1.25 mL, 10 mM). All reagents were added in the specified order. The growth of nanoparticles commenced by gently adding 0.5 mL of the seed solution to solution A. Following this, 5 mL of growth solution A was quickly transferred to solution B, with gentle mixing thereafter. Finally, 0.1 mL of solution B was added to growth solution C. Upon this addition, the color of solution C changed from clear to a deep magenta-purple within 30 min. The initial yield of spherical Au nanoparticles from this procedure was about 70%. After allowing

growth to proceed for 2 h, the final mixture was left undisturbed for 12 h. The supernatant was then carefully transferred via syringe to a clean beaker, increasing the purity of the Au nanoparticles to approximately 98%.

Subsequently, spherical Au nanoparticles with smooth surfaces were obtained through regrowth of the as-prepared Au nanoparticles followed by Au^{3+} oxidative etching[12]. The regrowth step was carried out as follows: 1 mL of $HAuCl_4 \cdot 3H_2O$ (10 mM) was mixed with 40 mL of cetylpyridinium chloride (10 mM) as the growth solution. Then, 30 mL of L-ascorbic acid (100 mM) and 5 mL of the as-prepared Au nanoparticles were added to the growth solution. The mixture was gently stirred in a 26 ℃ water bath for 30 min. After that, the mixture was centrifuged twice (8000 rpm, 12 min) to remove unreacted ions. The collected precipitate was resuspended in CTAB solution (50 mM), and its optical density (OD) was adjusted to 1.

Au^{3+}-mediated oxidative etching step: 16 μL of $HAuCl_4 \cdot 3H_2O$ (10 mM) was added to 5 mL of CTAB suspension with an optical density (OD) of 1, and the mixture was gently stirred in a water bath at 37 ℃ for 4 hours. Subsequently, the mixture was centrifuged once at 8000 rpm for 12 minutes. Water was then added, and the mixture was centrifuged twice at 8000 rpm for 10 minutes to remove unreacted ions, resulting in smooth spherical Au nanoparticles with an average radius of approximately 42 nm (Supplementary Fig. S2c). Furthermore, by adjusting the ratio of $HAuCl_4 \cdot 3H_2O$ to the as-prepared Au nanoparticles during the regrowth process, as well as varying the amount of $HAuCl_4 \cdot 3H_2O$ during the Au^{3+}-mediated oxidative etching process, smooth spherical Au nanoparticles of different sizes can be obtained (Supplementary Fig. S18).

Supplementary Figures

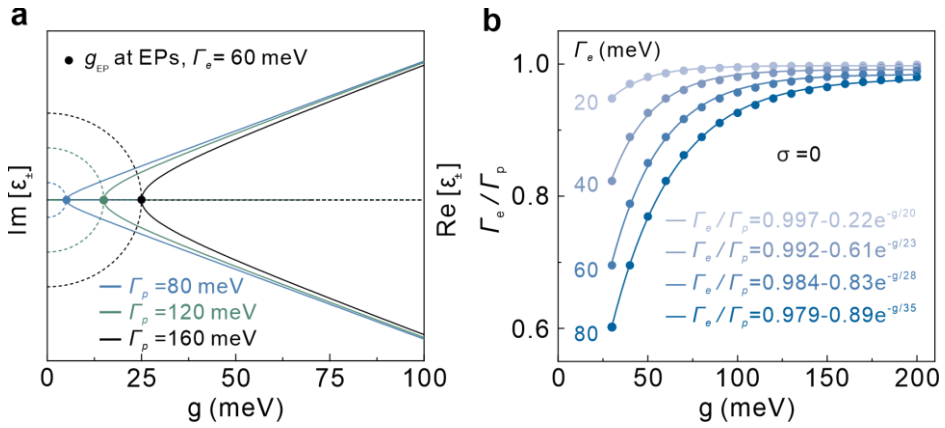

Figure S1. (a) Real (solid curves) and imaginary (dashed curves) parts of the eigenenergies as a function of g at resonance for three cases: Γ_p= 160 meV, Γ_p= 120 meV and Γ_p= 80 meV. **(b)** Dependence of the damping ratio Γ_e/Γ_p on the coupling strength g for different Γ_e values at σ = 0. Solid lines show exponential fits.

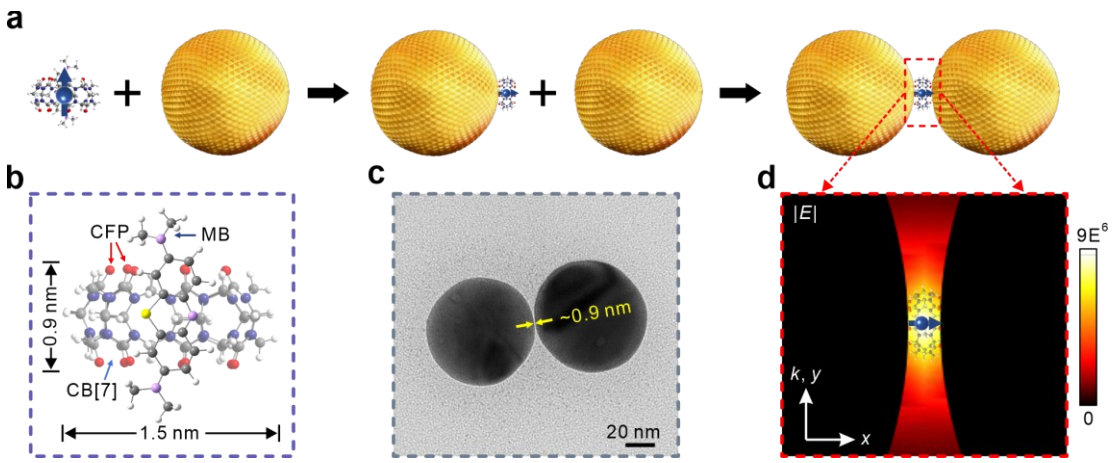

Figure S2. Precise positioning and alignment of a single MB molecule in Au NDC. **a,** Process flow to fabricate a hybrid Au NDC containing a single MB molecule with deterministic position and dipole alignment. **b,** Schematics of a single MB molecule embedded in a CB[7] cage and the single molecule can be integrated in the gap center of the Au NDC via the CB[7]. CFP: carbonyl-fringed portals. **c,** Transmission electron microscope (TEM) image of an Au NDC/CB[7]@single MB hybrid. **d,** Simulated electric field (EF) distributions of the gap plasmon mode confined in the Au NDC with a 0.9 nm gap.

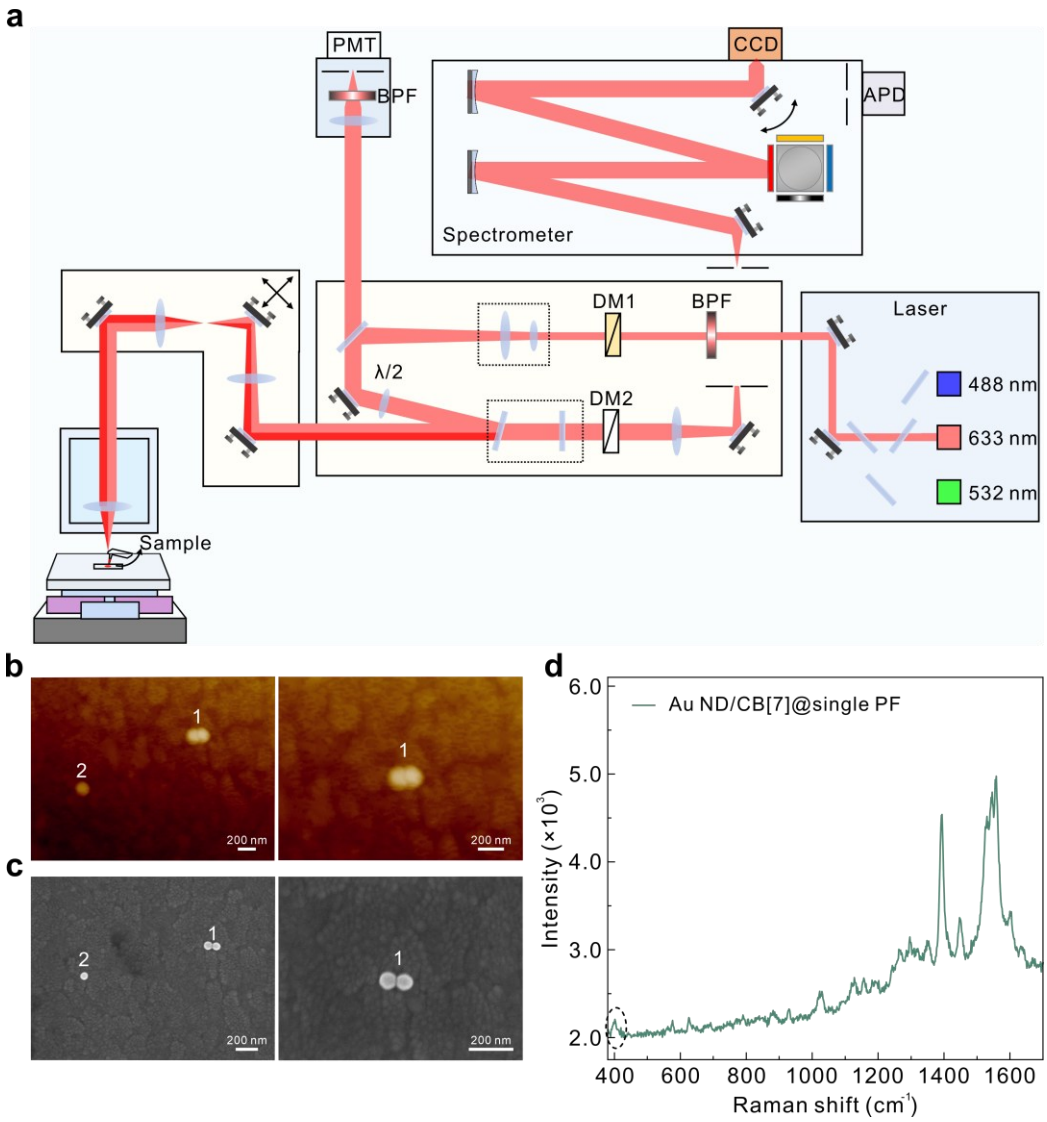

Figure S3. SERS measurement for single-molecule events in individual Au NDCs. **a,** Experimental system configuration for atomic force microscope-Raman (AFM-Raman) combined system. **b**, **c**, AFM images (**b**) and SEM images (**c**) of a measured Au NDC. **d,** SERS spectra obtained from the hybrid Au NDC sample in (**b**) or (**c**).

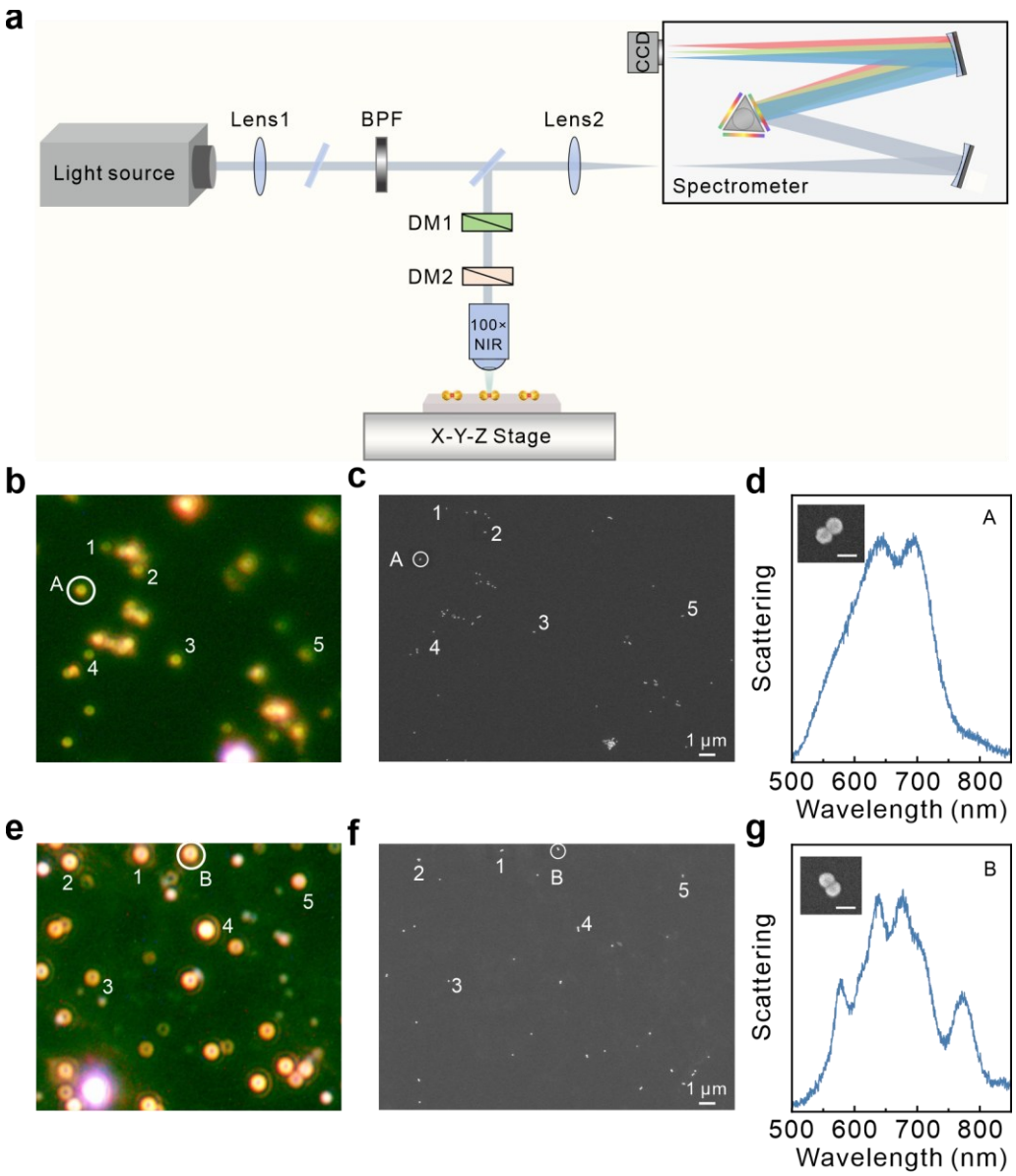

Figure S4. Dark-field scattering and corresponding SEM images of the measured samples on bulk SiO_2 and Si/SiO_2 photonic substrate. a, Experimental system configuration for dark-field scattering measurements. **b,** Dark-field scattering images of the measured Au NDC/CB[7]@single MB hybrids on bulk SiO_2 substrate. **c,** Corresponding SEM images of the measured samples in (**b**). **d,** Scattering spectrum and corresponding SEM image in a larger magnification (inset) and for the Au NDC/CB[7]@single MB hybrids marked in (**b**). **e,** Dark-field scattering images of the measured Au NDC/CB[7]@single MB hybrids on the Si/SiO_2 photonic substrate with t_{SiO_2} = 2.58 μm. **f,** Corresponding SEM images of the measured Au NDC/CB[7]@single MB hybrids in (**e**). **g,** Scattering spectrum and corresponding SEM image in a larger magnification (inset) and for the Au NDC/CB[7]@single MB hybrids marked in (**f**). The scale in the inset bar is 100 nm.

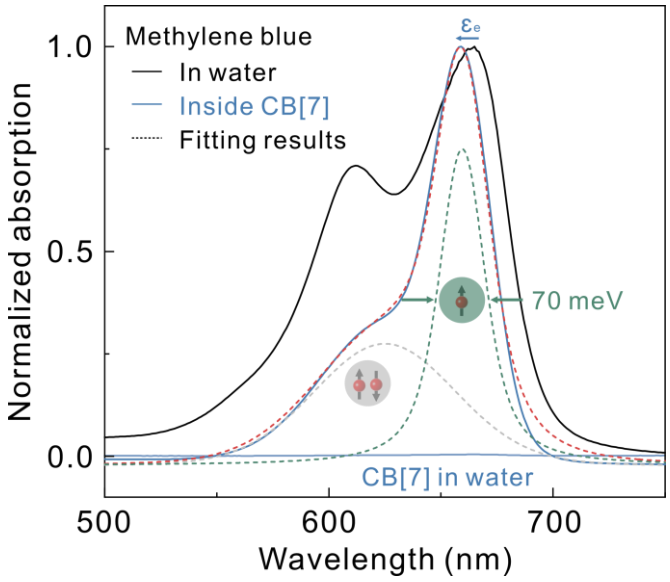

Figure S5. Absorption spectra of the MB molecules in aqueous solutions with and without CB[7]. Black line: Normalized absorption spectrum of the MB molecules in aqueous solutions without CB[7]. Blue line: Normalized absorption spectrum of MB molecules in water with CB[7]. The dashed lines are Lorentz fitted results, showcasing the MB monomer in CB[7] and dimer, respectively. The molar ratio of MB and CB[7] is 1: 2.

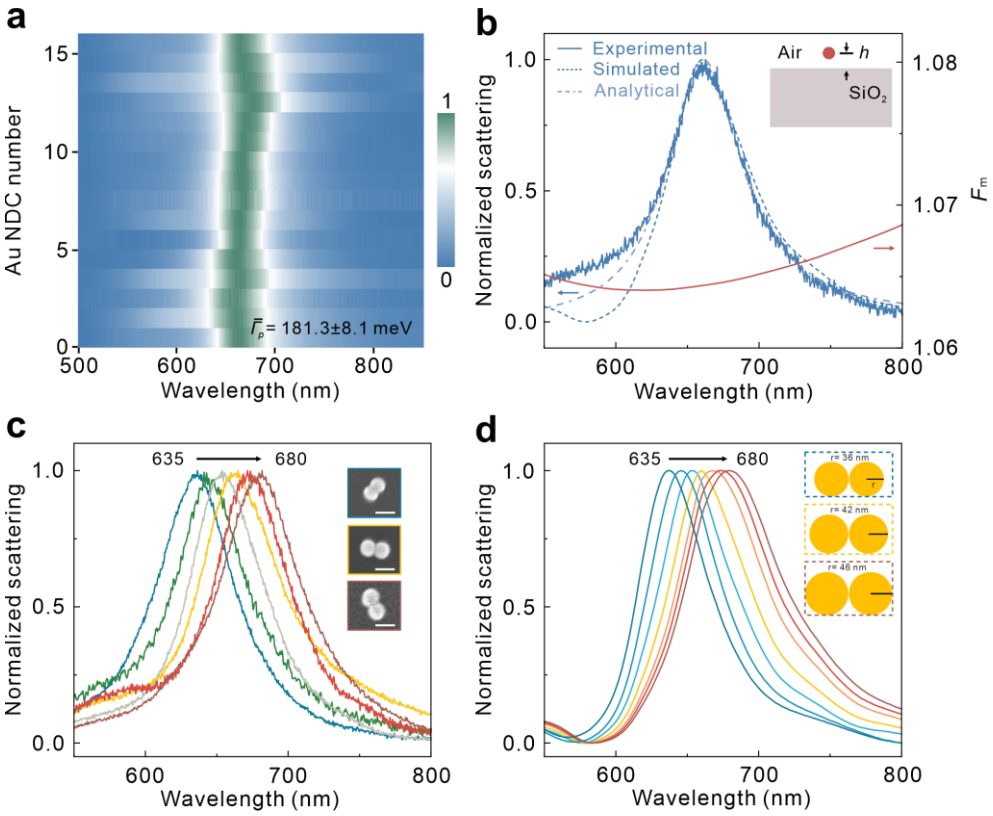

Figure S6. Experimental and simulated scattering spectra of the bare Au NDCs with different particle sizes. a, Representative scattering spectra of the individual bare Au NDCs on the bulk SiO_2 substrate. The mean value of $\bar{\Gamma}_p$ = 181.3 ± 8.1 meV can be obtained for the resonance wavelength at ~660-670 nm. **b,** Normalized scattering spectra of an Au NDC on the bulk SiO_2 substrate (solid blue line), the simulated result (dashed blue), and the analytical result (dot-dashed pale blue) calculated using Eq. (4) in the main text, with $F_m(\boldsymbol{r}, \omega, \hat{\boldsymbol{\mu}}_p) = C$. Red line: the F_m spectrum simulated at h = 42 nm above the bulk SiO_2 substrate. There are no OPs, we set $F_m(\boldsymbol{r}, \omega, \hat{\boldsymbol{\mu}}_p)$ as a constant (C). **c,** Normalized scattering spectra of individual bare Au NDCs with different particle sizes located on bulk SiO_2 substrate, showcasing the plasmon resonance wavelength varying from 635 to 680 nm. The insets give the SEM images of the measured samples related to the scattering spectra with the same line color as the box around the SEM images. The scale bar is 100 nm. **d,** Normalized scattering spectra of the bare Au NDCs with different sizes and a fixed gap distance of d = 0.9 nm, located on the bulk SiO_2 substrate. These spectra are simulated using the 3D-FEM (Supplementary Note 4).

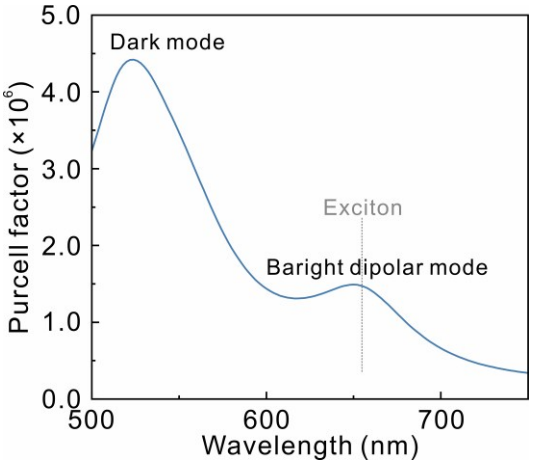

Figure S7. Purcell factor of the Au NDC with a gap distance of 0.9 nm. Purcell factor simulation of the Au NDC constructed by a single CB[7] molecule (d = 0.9 nm), with a classical electric dipole placed in the center of the gap at the position of maximum field and spontaneous emission rate plotted as a function of wavelength (Supplementary Note 3).

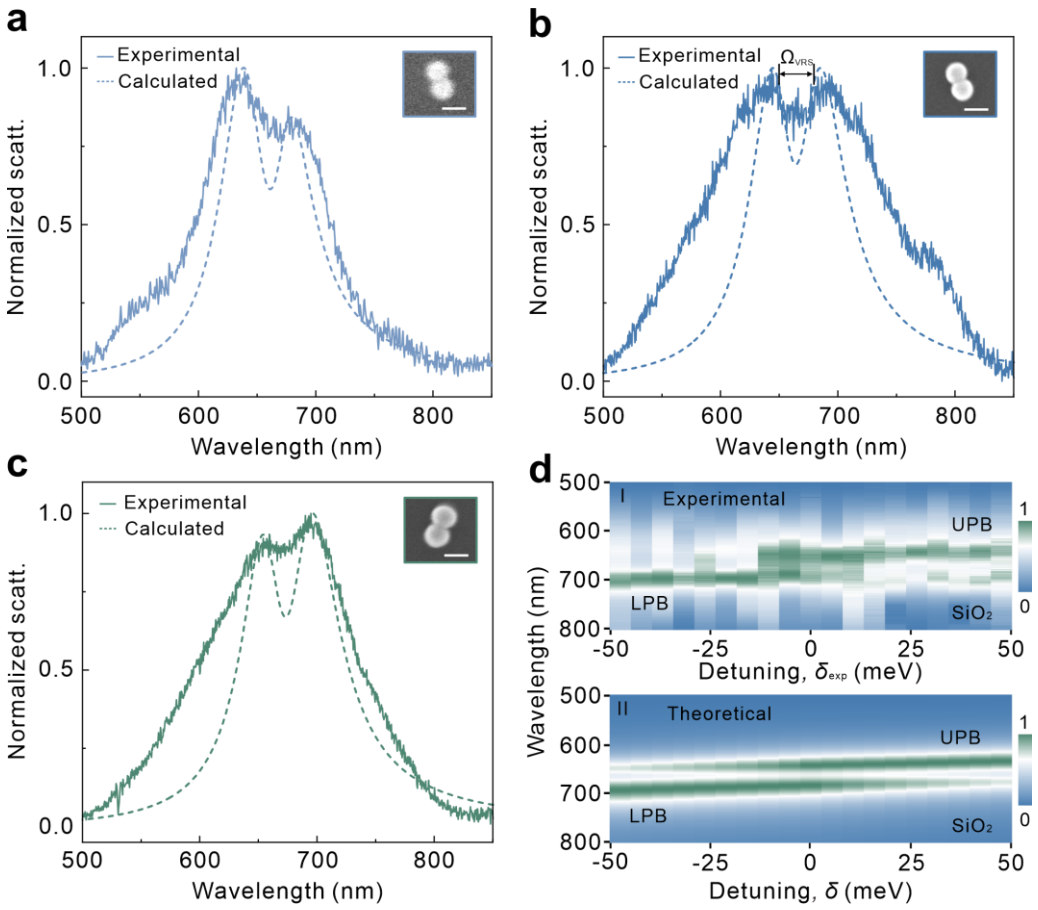

279

280 **Figure S8. Single-exciton strong coupling in individual Au NDC/CB[7]@single**
281 **MB hybrids with different detuning on bulk SiO_2. a-c**, Scattering spectra of three
282 individual Au NDC/CB[7]@single MB hybrids with different experimental detuning
283 (**a**) $\delta_{exp} > 0$, (**b**) $\delta_{exp} = 0$, and (**c**) $\delta_{exp} < 0$. The dashed curves show the theoretical
284 spectra of these strongly coupled systems calculated using Eq. (5) in the main text. The
285 insets show SEM images of the corresponding measured samples. The scale bar is 100
286 nm. **d,** (I) Normalized scattering spectra of the individual Au NDC/CB[7]@single MB
287 hybrids ordered according to the experimental detuning ($\delta_{exp} = \varepsilon_+ + \varepsilon_- - 2\varepsilon_e$). (II):
288 Normalized scattering spectra calculated using Eq. (5) in the main text, arranged by the
289 size of the theoretical detuning ($\delta = \varepsilon_p - \varepsilon_e$).

290

291

292

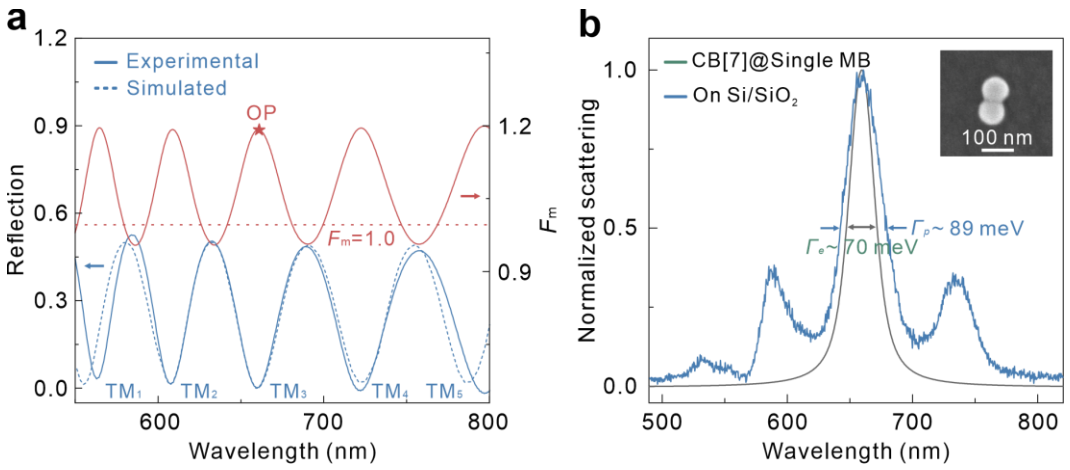

Figure S9. Plasmonic damping linewidth suppression through Si/SiO₂ photonic substrate with t_{SiO_2}= 2.58 μm. a, Measured (solid blue line) and simulated (dashed blue line) reflectance of the bare Si/SiO₂ photonic substrate with t_{SiO_2}= 2.58 μm. The solid red line is the F_m spectrum simulated at h = 42 nm above the substrate, **b,** Normalized scattering spectrum of bare Au NDC on the Si/SiO₂ photonic substrate with t_{SiO_2}= 2.58 μm, respectively. The gray line represents the fitted absorption spectrum of the CB[7]@single MB in water (Supplementary Fig. 5).

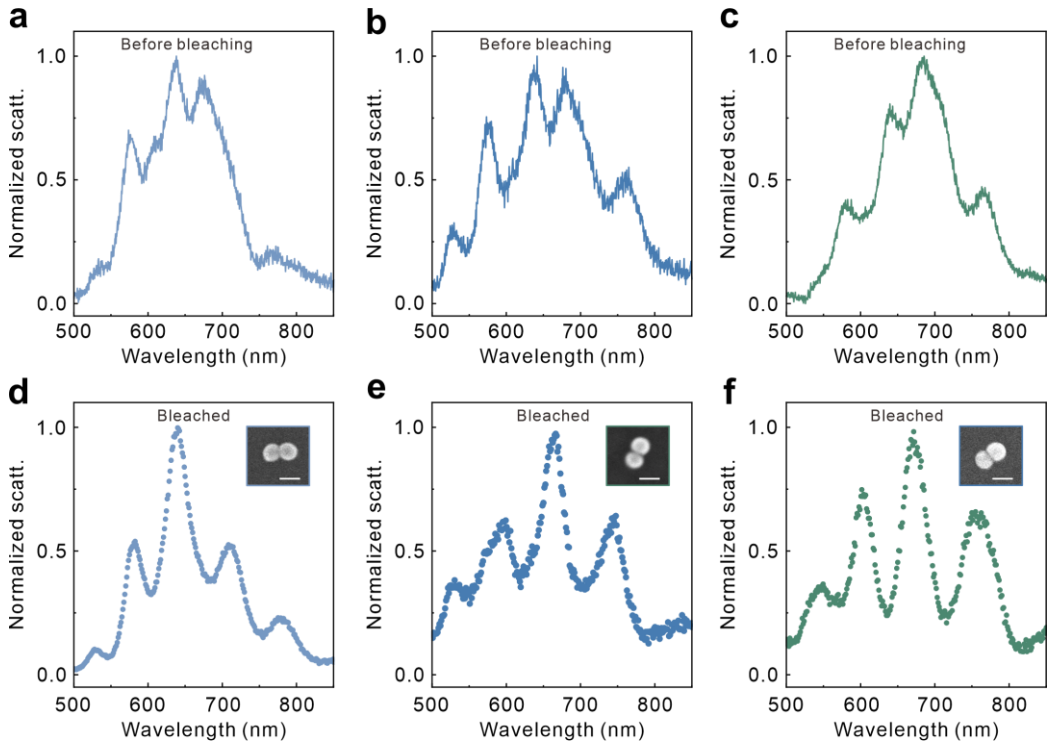

Figure S10. Photobleaching of the strongly coupled Au NDC/CB[7]@single MB hybrids. a-c, Normalized scattering spectra of individual Au NDC/CB[7]@single MB hybrids on Si/SiO₂ substrate (t_{SiO_2}= 2.58 μm). **d-f,** Normalized scattering spectra of the samples in (**a-c**) after photobleaching induced by laser illumination. The insets are SEM

images of the measured hybrid Au NDCs. The scale bar is 100 nm.

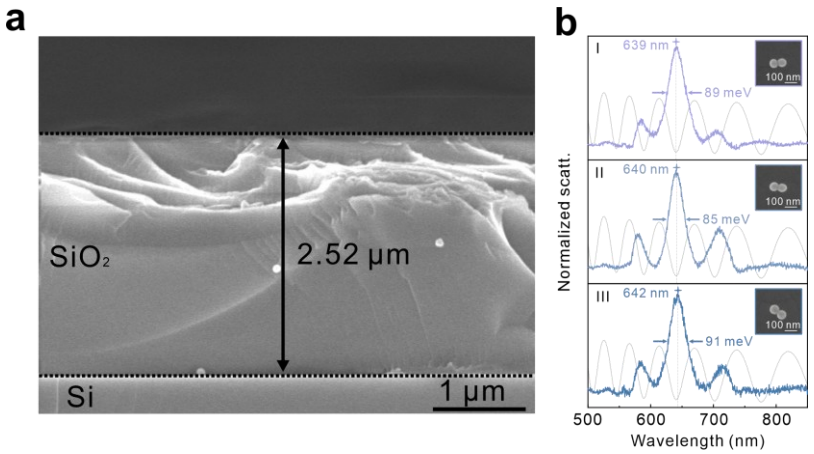

Figure S11. Normalized scattering spectra for three Au NDCs on a Si/SiO₂ photonic substrate with t_{SiO_2} = 2.52 μm. a, Side-view SEM image of the Si/SiO₂ photonic substrate with t_{SiO_2} = 2.52 μm. **b,** Normalized scattering spectra for three individual Au NDCs located on this Si/SiO₂ substrate. The dashed grey curves represent the experimental reflectance of the bare Si/SiO₂ substrate. The insets are corresponding SEM images for the measured Au NDCs, and the scale bar is 100 nm.

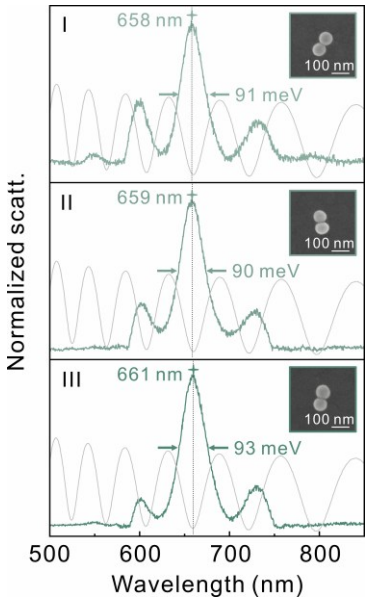

Figure S12. Normalized scattering spectra for three individual Au NDCs on a Si/SiO₂ photonic substrate with t_{SiO_2} = 2.58 μm. The side-view SEM image of this substrate can be seen in Fig. 3b of the main text. The dashed grey curves represent the experimental reflectance of the bare Si/SiO₂ substrate. The insets are corresponding SEM images for the measured Au NDC, and the scale bar is 100 nm.

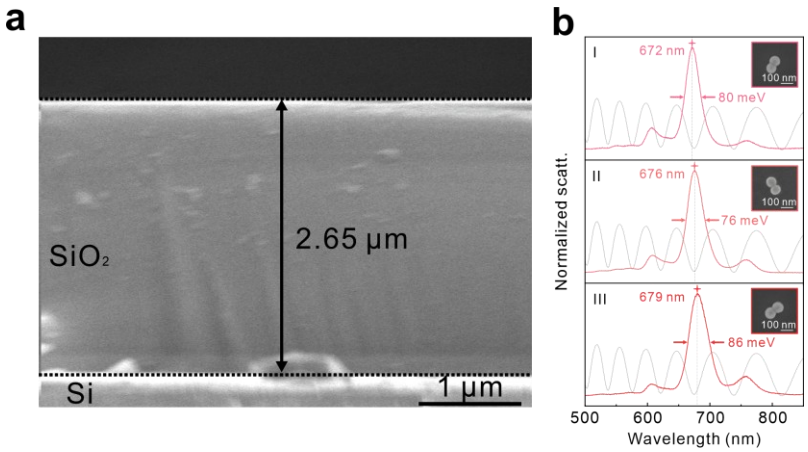

Figure S13. Normalized scattering spectra for three individual Au NDCs on a Si/SiO_2 photonic substrate with t_{SiO_2} = 2.65 μm. a, Side-view SEM image of the Si/SiO_2 photonic substrate with t_{SiO_2} = 2.65 μm. **b,** Normalized scattering spectra for three different Au NDCs located on the same Si/SiO_2 substrate. The dashed grey curves represent the experimental reflectance of the bare Si/SiO_2 substrate. The insets are corresponding SEM images for the measured Au NDCs, and the scale bar is 100 nm.

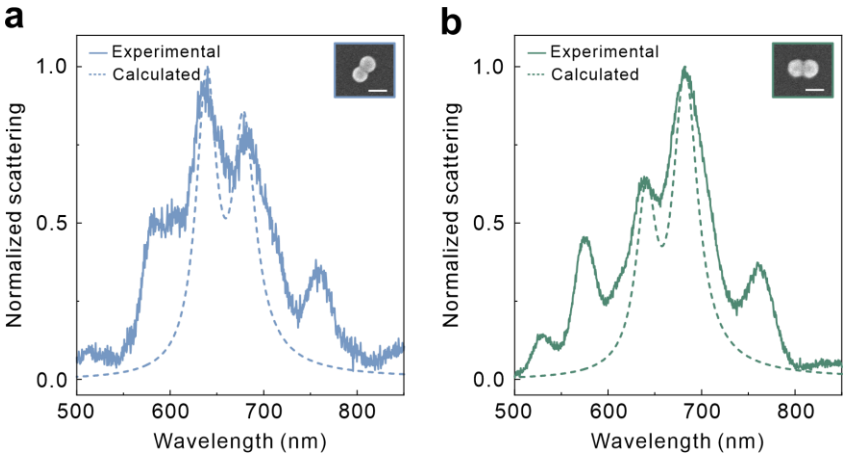

Figure S14. Au NDC/CB[7]@single MB hybrids with different detuning on the Si/SiO_2 photonic substrate with t_{SiO_2} of about 2.58 μm. a, **b**, Normalized scattering spectra of Au NDC/CB[7]@single MB hybrids with different experimental detuning **(a)** $\delta_{exp} > 0$ and **(b)** $\delta_{exp} < 0$. The dashed curves are theoretical results calculated using Eq. (5) in the main text. The insets show SEM images of the corresponding measured samples, and the scale bar is 100 nm.

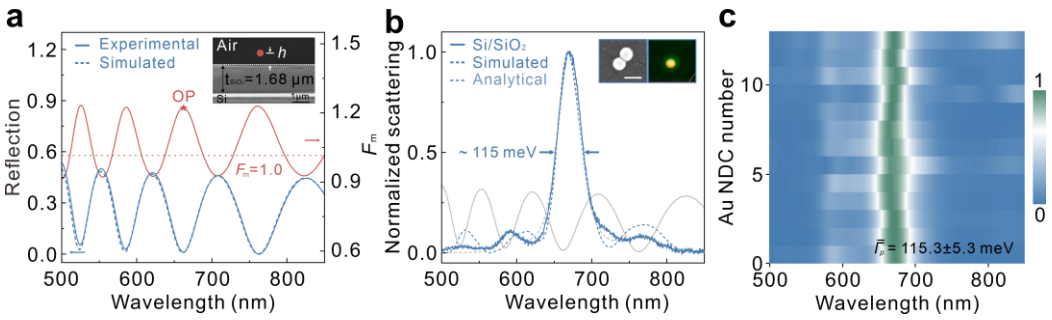

334

335 **Figure S15. Plasmonic damping linewidth suppression through Si/SiO₂ photonic**
336 **substrate with t_{SiO_2} = 1.68 μm. a**, Measured (solid blue line) and simulated (dashed
337 blue line) reflectance of the bare Si/SiO₂ photonic substrate with t_{SiO_2} = 1.68 μm. The
338 solid red line is the F_m spectrum simulated at h = 42 nm above the substrate. The inset
339 is the side-view SEM image of this substrate. **b**, Normalized scattering spectra of an Au
340 NDC on the photonic substrate (solid blue line), the simulated result (dashed blue), the
341 analytical result (dot-dashed pale blue) calculated using Eq. (4), and measured
342 reflectance of the bare photonic substrate (solid gray). Insets: SEM image (left) and
343 dark-field image (right) of the measured Au NDCs, respectively. The scale bar is 100
344 nm. **c,** Scattering spectra of the individual Au NDCs with the resonance wavelength at
345 660-670 nm measured on this photonic substrate. The mean value of $\bar{\Gamma}_p$ = 115.3 ± 5.3
346 meV can be obtained.

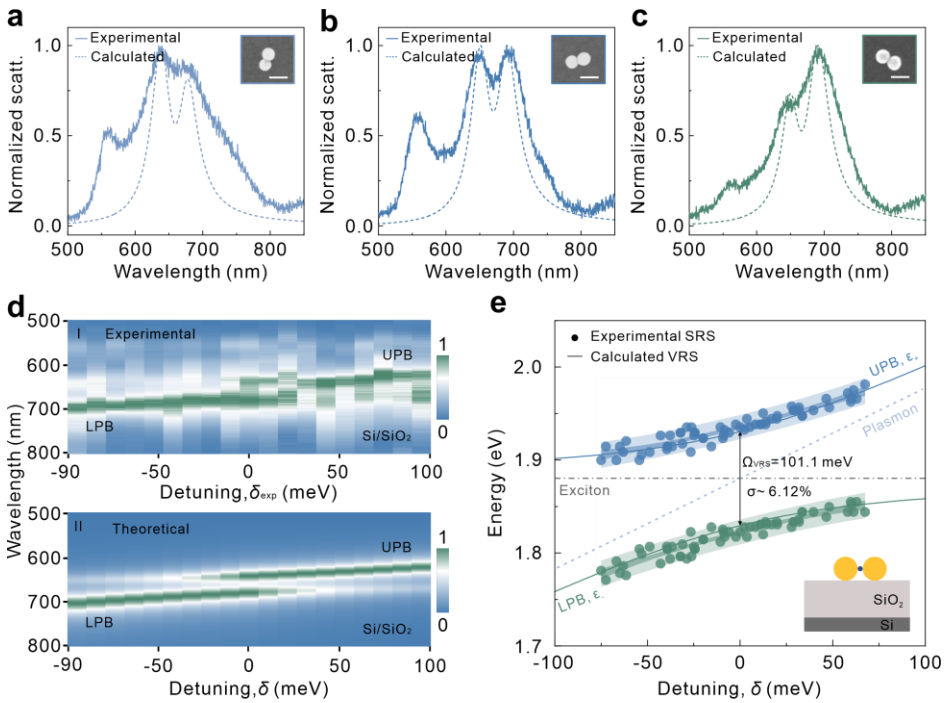

347

348 **Figure S16. Single-exciton strong coupling in individual Au NDC/CB[7]@single**
349 **MB hybrids on Si/SiO₂ substrate with t_{SiO_2} of about 1.68 μm. a-c**, Normalized

scattering spectra of three individual Au NDC/CB[7]@single MB hybrids with different experimental detunings of (**a**) $\delta_{exp} > 0$, (**b**) $\delta_{exp} = 0$, and (**c**) $\delta_{exp} < 0$. The dashed curves show the theoretical spectra of the strongly coupled systems calculated using Eq. (5) in the main text. The insets show SEM images of the corresponding measured samples. The scale bar is 100 nm. **d,** (I) Normalized scattering spectra of individual Au NDC/CB[7]@single MB hybrids measured on the Si/SiO_2 substrates with t_{SiO_2} of about 1.68 μm, ordered according to the experimental detuning δ_{exp}. (II) Normalized scattering spectra calculated using Supplementary Eq. (5), arranged by the size of the theoretical detuning (δ). **e,** Energy dispersions of the mixed states extracted from individual Au NDC/CB[7]@single MB hybrids measured on the Si/SiO_2 photonic substrate with t_{SiO_2} of about 1.68 μm. The solid lines are theoretical energy dispersions calculated using Eq. (2). The dark shaded area represents the 95% confidence interval.

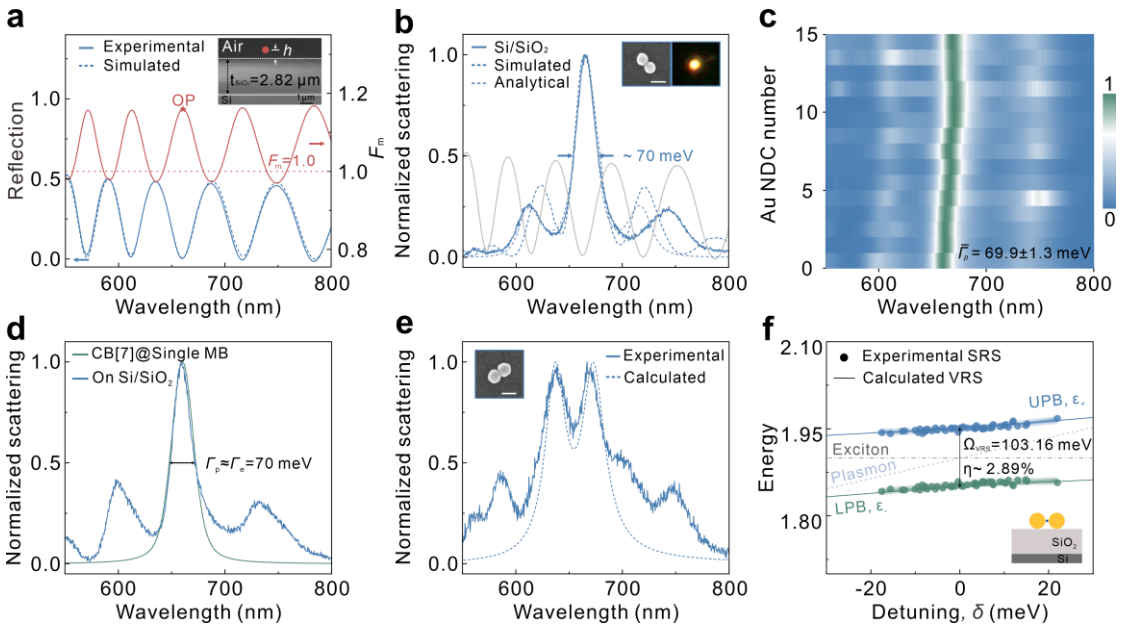

Figure S17 Plasmonic damping linewidth suppression through Si/SiO_2 photonic substrate with t_{SiO_2}= 2.82 μm. a, Measured (solid blue line) and simulated (dashed blue line) reflectance of the bare Si/SiO_2 photonic substrate with t_{SiO_2}= 1.68 μm. The solid red line is the F_m spectrum simulated at h = 42 nm above the substrate. The inset is the side-view SEM image of this substrate. **b**, Normalized scattering spectra of an Au NDC on the photonic substrate (solid blue line), the simulated result (dashed blue), the analytical result (dot-dashed pale blue) calculated using Eq. (4), and measured reflectance of the bare photonic substrate (solid gray). Insets: SEM image (left) and dark-field image (right) of the measured Au NDCs, respectively. The scale bar is 100 nm. **c,** Scattering spectra of the individual Au NDCs with the resonance wavelength at 660-670 nm measured on this photonic substrate. The mean value of $\bar{\Gamma}_p$ = 69.9 ± 1.3

meV can be obtained. **d,** Normalized scattering spectrum of bare Au NDC on the Si/SiO_2 photonic substrate witht_{SiO_2}= 2.82 μm, respectively. The gray line represents the fitted absorption spectrum of the CB[7]@single MB in water (Supplementary Fig. 5). **e,** Normalized scattering spectra of an Au NDC/CB[7]@single MB hybrid on Si/SiO_2 photonic substrate. The dashed curve is the theoretical prediction calculated using Eq. (5). **f,** Energy dispersions of the mixed states extracted from individual Au NDC/CB[7]@single MB hybrids measured on the Si/SiO_2 photonic substrate with t_{SiO_2} of about 2.82 μm. The solid lines are theoretical energy dispersions calculated using Eq. (2). The dark shaded area represents the 95% confidence interval.

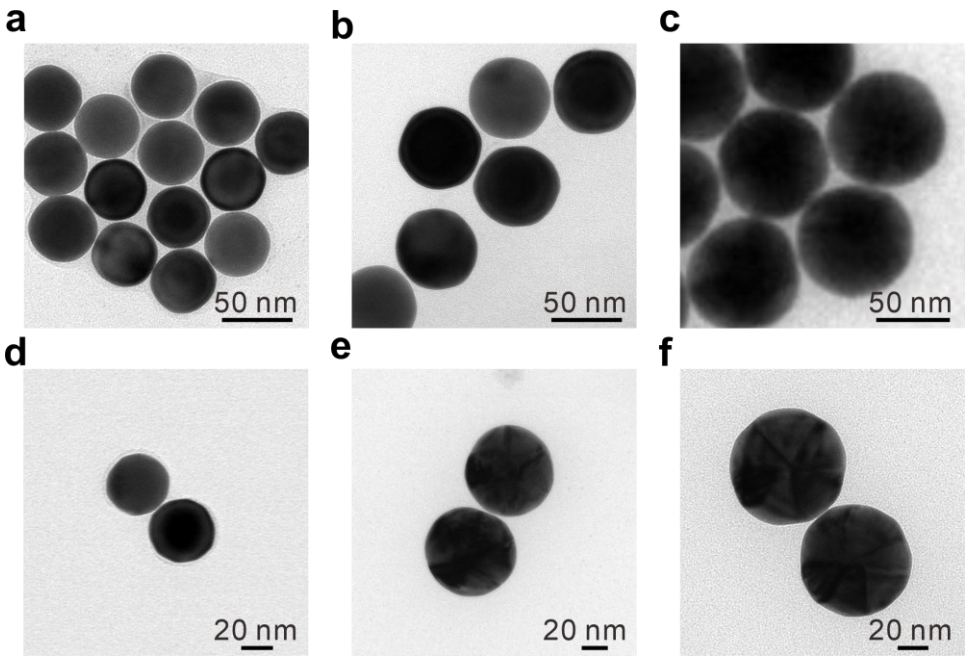

Figure S18 Morphology characterization of Au nanoparticles with different sizes. **a-c** TEM images of the spherical Au nanoparticles with different radii of (**a**) 22.6 ± 1.3nm, (**b**) 30.1 ± 2.2 nm, and (**c**) 40.4 ± 2.6 nm. **d-e** TEM images of Au NDCs prepared using the Au nanoparticles with a radius of ~20 nm, 30 nm, and 40 nm.

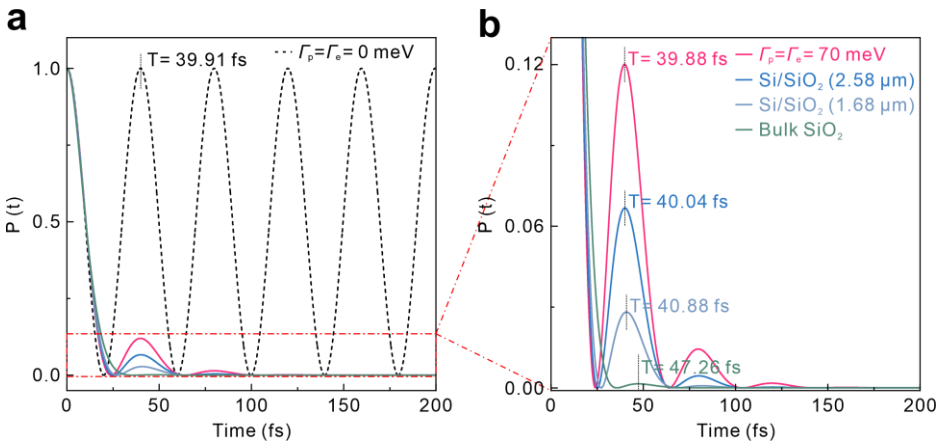

Figure S19. Vacuum Rabi oscillations calculated in Au NDC/CB[7]@single MB hybrids positioned on bulk SiO_2 and Si/SiO_2 photonic substrates with different t_{SiO_2}. **a**, Calculated upper-state dynamic evolutions of the initially excited emitter in the lossy Au NDCs, with varying Γ_p, correspond to the cases illustrated in Fig. 4b of the main text. The other parameters are same as those used in Fig. 4c in the main text. The dashed line is calculated for the ideal case of $\Gamma_p = \Gamma_e = 0$, and the red line is calculated at $\Gamma_p = \Gamma_e = 70$ meV. **b**, Enlarged view of the area within the dashed box in (**a**). The dashed line is not given.

Supplementary Tables

Table S1. Calculated V_{eff} and other parameters for the Au NDCs on different substrates.

Substrate	λ (nm)	Γ_p (nm)	V_{eff} (nm^3)	V_{EP} (meV)	g (meV)	Ω_{VRS} (meV)
bulk SiO_2	660	181	52.5	27.75	51.82	87.5
Si/SiO_2 (t_{SiO_2}=1.68 μm)	661	115	51.4	11.25	51.83	101.1
Si/SiO_2 (t_{SiO_2}=2.58 μm)	661	89	51.3	4.75	51.87	103.2
Si/SiO_2 (t_{SiO_2}=2.82 μm)	662	70	51.3	0	51.82	103.6

Note that, since the Au NDC has a ~0.9-nm gap, the plasmonic electric field $\boldsymbol{E}_p(\boldsymbol{r},\omega)$ and the corresponding energy density are predominantly distributed in the nanogap between the

nanoparticles. Thus, the permittivity ($\epsilon(\boldsymbol{r},\omega)$) is still dominated by the that in the nanogap in the nanodimer, where $\epsilon(\boldsymbol{r},\omega) = 1.0$ for air. Therefore, $V_{\mathrm{eff}} = V_{\mathrm{m}} \times \epsilon(\boldsymbol{r}) \approx V_{\mathrm{m}}$[13] was used in our V_{eff} calculations.

Supplementary References

1. Manjavacas, A., García de Abajo, F. J. & Nordlander, P. Quantum plexcitonics: strongly interacting plasmons and excitons, *Nano Lett.* **11**, 2318–2323 (2011).

2. Liu, R. et al. Strong light-matter interactions in single open plasmonic nanocavities at the quantum optics limit. *Phys. Rev. Lett.* **118**, 237401 (2017).

3. Zubarev, D. N. Double-time Green functions in statistical physics. *Sov. Phys. Usp.* **3**, 320 (1960).

4. Du, R. et al. How to obtain the correct Rabi splitting in a subwavelength interacting system. *Nano Lett.* **23**, 444–450 (2023).

5. Aspnes, D. E. & Studna, A. A. Dielectric functions and optical parameters of si, ge, gap, gaas, gasb, inp, inas, and insb from 1.5 to 6.0 eV. *Phys. Rev. B* **27**, 985 (1983).

6. Rodríguez-de Marcos, L. V., Larruquert, J. I., Méndez, J. A., et al. Self-consistent optical constants of SiO_2 and Ta_2O_5 films. *Opt. Mater. Express* **6**, 3622-3637 (2016).

7. Johnson, P. B. & Christy, R.W. Optical constants of the noble metals. *Phys. Rev. B* **6**, 4370 (1972).

8. Chikkaraddy, R. et al. Single-molecule strong coupling at room temperature in plasmonic nanocavities. *Nature* **535**, 127–130 (2016).

9. Heintz, J. et al. Few-molecule strong coupling with dimers of plasmonic nanoparticles assembled on DNA. *ACS Nano* **15**, 14732−14743 (2021).

10. Liu, R. et al. On-demand shape and size purification of nanoparticle based on surface area. *Nanoscale* **6**, 13145–13153 (2014).

11. Millstone, J. E. et al. Iodide ions control seed-mediated growth of anisotropic gold nanoparticles. *Nano Lett*. **8**, 2656–2659 (2008).

12. O'Brien, M. N. et al. Uniform circular disks with synthetically tailorable diameters: Two dimensional nanoparticles for plasmonics. *Nano Lett*. **15**, 1012–1017 (2015).

13. Wang, X. H., Wang, R., Gu, B. Y. & Yang, G. Z. Decay distribution of spontaneous

emission from an assembly of atoms in photonic crystals with pseudogaps. *Phys. Rev. Lett*. **88**, 093902 (2002).